RSC Advances

PAPER

View Article Online
View Journal | View Issue

Cite this: *RSC Adv.*, 2021, **11**, 35893

NIR luminescent detection of quercetin based on an octanuclear Zn(II)–Nd(III) salen nanocluster†

Mengyu Niu,[ab] Xiaoping Yang,*[ab] Yanan Ma,[ab] Chengri Wang[ab] and Desmond Schipper[c]

Received 28th August 2021
Accepted 30th October 2021

DOI: 10.1039/d1ra06494k

rsc.li/rsc-advances

A NIR luminescent octanuclear Zn(II)–Nd(III) nanocluster **1** was constructed by the use of a salen-type Schiff base ligand. **1** exhibits a lanthanide luminescent response to Que with high sensitivity. The quenching constant of Que to the lanthanide emission is 2.6×10^4 M^{-1}, and the detection limit of **1** to Que is 2.5 μM. The response behavior of **1** to Que is not affected by the existence of some potential interferents such as biomolecules.

Introduction

Recently, fluorescence probes have received much attention due to their applications in the detection of various analytes with high sensitivity and selectivity, rapid response, and convenient utilization.[1–5] Among all kinds of target objects, quercetin (Que, 3,3′,4′,5,7-penta-hydroxy-flavone) is a kind of flavonoid existing extensively in vegetables, fruits, beverages and herbal medicines, and is a typical active antioxidant with an important role in the treatment of some cardiovascular diseases and prevention of biological cell degradation.[6–8] Many traditional analytical techniques, such as chromatography, spectrophotometry, and capillary electrophoresis, have been used to detect Que.[9–11] The fluorescence probes for the detection of Que mainly focus on quantum dots (QDs)[12] and carbon nanodots (CNDs).[13] Lanthanide complexes may display interesting visible and near-infrared (NIR) emissions with sharp emission spectra, large antenna-generated shifts and long lifetimes. Currently, Bin Zhao *et al.* first reported a visible luminescent sensor of Que based on a Tb(III)-based metal–organic framework (Tb-MOF).[14] Heterometallic d-4f complexes with Nd(III), Er(III) and Yb(III) ions can show superior NIR luminescence properties due to the efficient transfer energy from the light-absorbing units containing d-block metal ions such as Zn^{2+},[15] Cd^{2+},[16] Ru^{2+},[17] Pt^{2+},[18] and Cr^{2+},[19] to lanthanide ions. However, so far there are few reports on the use of polynuclear d-4f complexes for the NIR luminescent detection of Que.

Salen-type Schiff bases are typical ligands used in the construction of luminescent d-4f complexes.[20,21] Our recent studies have focused on the construction of lanthanide complexes with luminescent response toward small molecules and ions.[22–25] In this work, we report the construction of an octanuclear d-4f complex $[Zn_6Nd_2L_4(OAc)_2(DMF)EtOH]$ (**1**) from a Schiff base ligand *N*,*N*′-bis(3-hydroxysalicylidene)(4-methoxyphenylene)-1,2-diamine (H_4L, Scheme 1), which has a phenyl backbone. Compared with visible fluorescence, lanthanide NIR luminescence has advantages in the detection of biological system, due to the low absorption of biological matrixes in 1000–1700 nm. Interestingly, **1** shows NIR Nd(III) emission and exhibits high luminescent response to Que.

Results and discussion

Synthesis and crystal structure of the Zn(II)–Nd(III) nanocluster

The salen-type Schiff base ligand H_4L was synthesized from the reaction of 2,3-dihydroxybenzaldehyde and 4-methoxy-*o*-phenylenediamine (ESI†).[26] **1** was synthesized from the reaction of H_4L with $Nd(OAc)_3 \cdot 4H_2O$ and $Zn(OAc)_2 \cdot 2H_2O$. The molecular dimensions of **1** are about 1.1 × 1.6 × 1.8 nm (Fig. 1). In **1**, six Zn(II) and two Nd(III) ions are coordinated with four Schiff base ligands. Four Zn(II) ions are located in the N_2O_2 cavities of the

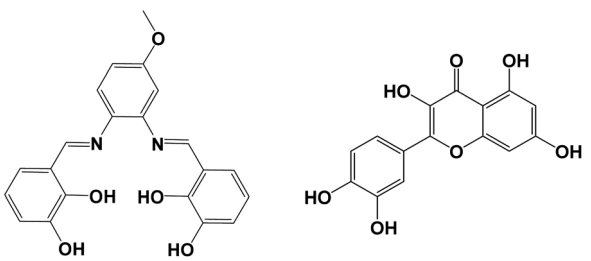

Scheme 1 The structures of salen-type Schiff base ligand H_4L (left) and Que (right).

[a]College of Chemistry and Materials Engineering, Wenzhou University, Wenzhou 325035, China

[b]Zhejiang Key Laboratory of Carbon Materials, Wenzhou 325035, China. E-mail: xpyang@wzu.edu.cn

[c]Department of Chemistry and Biochemistry, The University of Texas at Austin, 1 University Station A5300, Austin, Texas, 78712, USA

† Electronic supplementary information (ESI) available: Experimental and characterization details and additional figures. CCDC 2102148 for **1**. See DOI: 10.1039/d1ra06494k

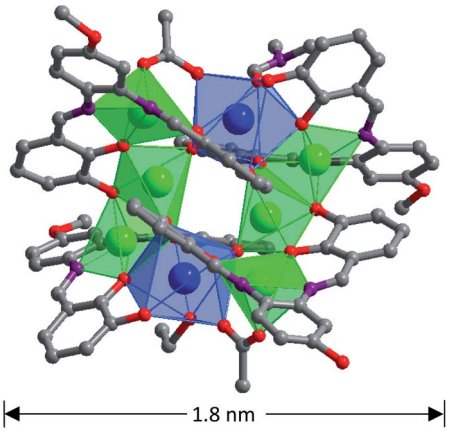

Fig. 1 The crystal structure of **1** (Zn(II): green; Nd(III): blue).

Schiff base ligands with a square based pyramidal geometry, while other two Zn(II) ions are coordinated with phenolic oxygen atoms of the ligands with a tetrahedral geometry. Each Nd(III) ion is bound to two O_2O_2 donor sets of the ligands, and the coordination number is eight. Each Nd(III) ion is surrounded by eight O atoms from three Schiff base ligands, one OAc^- anion and one solvent molecule EtOH (or DMF). The neighboring Zn(II) and Nd(III) ions are bridged by the phenolic oxygen atoms of four Schiff base ligands and two OAc^- anions, with an average separation of 3.76 Å. The bond lengths of Nd–O, Zn–O and Zn–N are 2.28–2.52 Å, 1.91–2.08 Å and 1.99–2.18 Å, respectively. Intramolecular π–π stacking interactions exist between the phenyl rings of Schiff base ligands (distances: 3.371 Å to 3.750 Å),[27,28] which helps the formation of **1**. Compared with other reported d-4f complexes with similar salen-type conjugated Schiff base ligands,[15,20,21,29] the Zn(II) ions in **1** are not only bound to the N_2O_2 donor sets of the ligands but also to their O_2O_2 sets. In Fig. 2, one image of scanning electron microscopy (SEM) displays the crystalline nature of **1**, and in energy dispersive X-ray (EDX) spectroscopy the molar ratio of Zn/Nd is about 3, consistent with its structure. The measured powder XRD pattern of **1** is similar to the simulated one generated from the crystal structure, indicating the purity of the solid product (Fig. S3†). Thermogravimetric analysis indicates that **1** loses about 3% weight before 100 °C, due to the escaping of uncoordinated solvent molecules such as MeOH, EtOH and H_2O in the sample. **1** starts to decompose from about 180 °C (Fig. S4†), which is also confirmed by the melting point measurement (see Experimental section).

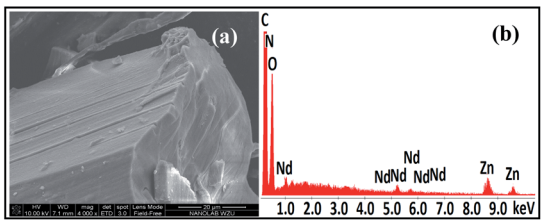

Fig. 2 The image of scanning electron microscopy (a) and energy dispersive X-ray spectroscopy (b) of **1**.

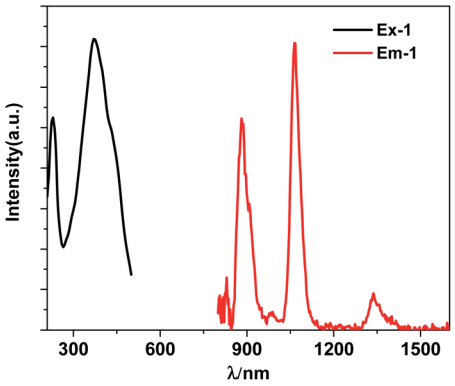

Fig. 3 The excitation (λ_{em} = 1064 nm) and NIR lanthanide emission (λ_{ex} = 370 nm) spectra of **1** (30 μM) in CH_3CN.

Photophysical properties and NIR luminescent response to Que

The free H_4L has three bands at 214 nm, 276 nm and 339 nm, which are assigned to n → π* or π → π* transitions associated with imine and phenyl functions of the Schiff base ligand. These bands are red-shifted in **1** due to the disturbance of metal ions in the structure (Fig. S7†). Upon the excitation in ligand-centered absorption band, **1** displays the NIR luminescence of Nd(III) ($^4F_{3/2} \rightarrow {}^4I_{j/2}$ transitions, j = 9, 11 and 13) at 880, 1064 and 1337 nm (Fig. 3). The emission lifetime (τ) is 5.6 μs (Fig. S8†), so the intrinsic quantum yield (Φ_{Ln}) of Nd(III) is calculated to be 2.2%, using equation $\Phi_{Ln} = \tau/\tau_0$ (τ_0 = 250 μs, the natural lifetime of Nd(III)).[30] The whole luminescence quantum yield (Φ_{em}) of **1** is 0.14%, thus, the energy transfer efficiency ($\eta_{sens} = \Phi_{em}/\Phi_{Ln}$) from the Schiff base ligands to Nd(III) ions can be calculated as 6.4%.[31]

The NIR luminescent sensing behaviour of **1** to Que was studied in CH_3CN. The results show that, as the concentrations of added Que increase, the intensities of lanthanide luminescence of **1** are decreased gradually (Fig. 4). The quenching constant (K_{SV}) of Que to the lanthanide emission is calculated to be 2.6 × 10^4 M^{-1}, by using Stern–Volmer equation.[32] Also, the limit of detection (LOD = 3σ/K_{SV} (ref. 33)) of **1** to Que is obtained to be 2.5 μM, which is among the lowest ones reported for the

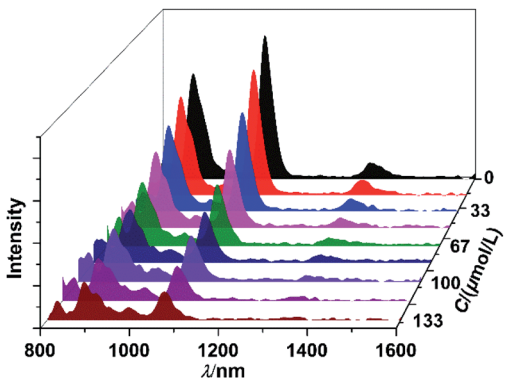

Fig. 4 The quenching of NIR luminescence of **1** (30 μM) to the addition of Que with different concentrations in CH_3CN.

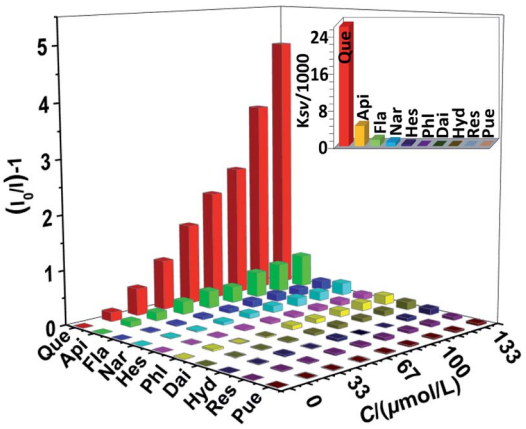

Fig. 5 The lanthanide luminescence quenching of **1** (30 μM) at 1064 nm to Que and interferents in CH_3CN. Inset: the K_{SV} values for the luminescence quenching of **1**. (λ_{ex} = 370 nm).

fluorescent detection of Que so far.[12–14,34–37] It is noticeable that, the shapes of NIR emission peaks of **1** are same before and after the addition of Que (Fig. 4). Meanwhile, conductivity study confirms that **1** is neutral in CH_3CN, in accordance with the crystal structure. These results suggest that **1** is stable during the sensing experiments.

To assess the response selectivity of **1** to Que in biological system, we investigated its sensing behaviour to potential biomolecule interferents such as apigenin (Api), flavanone (Fla), naringin (Nar), hesperidin (Hes), phloroglucinol (Phl), daidzein (Dai), hydroquinone (Hyd), resorcinol (Res) and puerarin (Pue) (Scheme S1†). Compared to Que, the addition of these biomolecules causes much smaller changes to the lanthanide emission of **1** (Fig. 5 and S9†). For instance, the lanthanide emission quenching of **1** caused by 60 μM biomolecules is less than 30% (Fig. S9†), indicating the sensing selectivity of **1** to Que. Additionally, the response behaviour of **1** to Que in the presence of the interferents was examined. The results show that the quenching of the lanthanide emission of **1** aroused by Que is not affected by the existence of the interferents (Fig. 6). The luminescence selectivity of **1** to Que was further confirmed

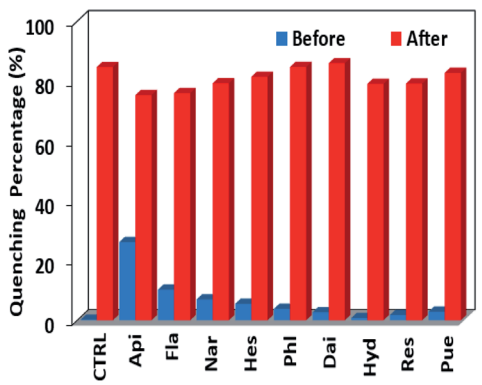

Fig. 6 The lanthanide luminescence quenching of **1** (30 μM) at 1064 nm before and after the addition of Que (60 μM) with the existence of the interferents (60 μM) in CH_3CN.

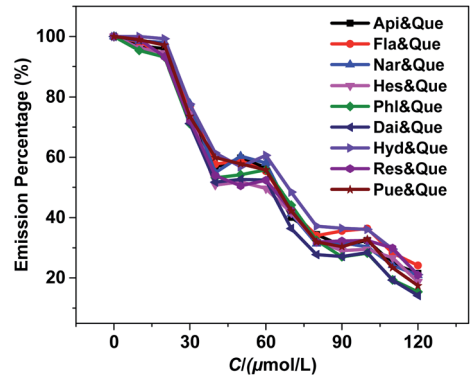

Fig. 7 The luminescence intensity changes of **1** (30 μM) with the step-by-step addition of interferents and Que (10 μM each time).

by the step-by-step addition of the interferents. For instance, the luminescence decreases slowly when Api is added twice firstly (Fig. 7). While, it decreases fast by the subsequent addition of equal amount of Que. This trend happens again in the following additions of Api and Que, suggesting the high selectivity of **1** to Que even in the existence of the interferents.

In **1**, the Schiff base ligands can absorb and transfer energy to Nd(III) ions, resulting in the lanthanide luminescence ("antenna effect", Scheme 2).[38] It is noticeable that, Que has a much higher absorption coefficient at λ_{ex} = 370 nm than **1** (1.18×10^5 M^{-1} cm^{-1} *vs.* 0.21×10^5 M^{-1} cm^{-1}, Fig. 8 and S7†). Thus, the added Que can compete with **1** for the energy absorption at λ_{ex}, resulting in the quenching of lanthanide luminescence ("inner filter effect", Scheme 2).[39–41] As shown in Fig. 8, the absorptions of biomolecule interferents at λ_{ex} are much weaker than Que, and they have little effect on the lanthanide luminescence of **1**. The "inner filter effect" of Que to the lanthanide luminescence can be confirmed by comparing the quenching constants of Api and other biomolecule interferents. The absorption coefficient of Api at λ_{ex} is 0.15×10^5 M^{-1} cm^{-1}, which is higher than those of other interferents (less than 0.07×10^5 M^{-1} cm^{-1}) (Fig. 8), thus, Api can absorb

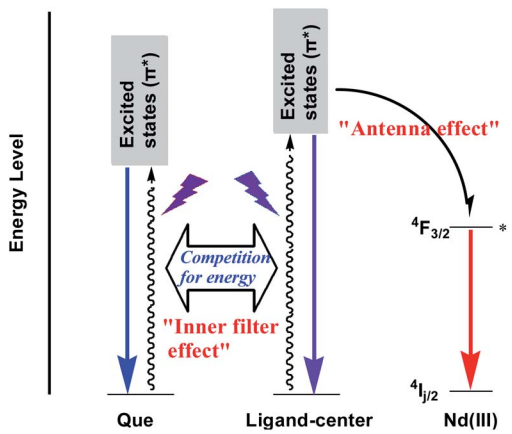

Scheme 2 The "antenna effect" of the Schiff base ligand and "inner filter effect" of Que to the lanthanide luminescence in **1**.

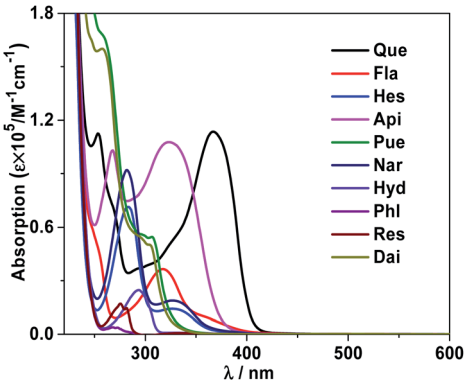

Fig. 8 Absorption spectra of Que and interferents in CH_3CN at room temperature.

more light energy than other interferents. Unsurprisingly, Api also shows larger K_{SV} value (0.44×10^4 M^{-1}) than other interferents (less than 0.13×10^4 M^{-1}), demonstrating the "inner filter effect" to the lanthanide luminescence. Furthermore, the addition of Que results in the quenching of visible ligand-centered emission of **1** at 545 nm (Fig. S10†). This is also due to the decrease of excitation energy of Schiff base ligands caused by the "inner filter effect" of Que.

Experimental

Materials and general methods

All chemical materials were obtained from commercial sources and directly used without further purified. The Schiff base ligand and the lanthanide complex were synthesized using Schlenk system. Elemental analyses were performed on a EURO EA3000. Melting points were obtained on an XT-4 electro-thermal micromelting point apparatus. IR spectra of the Schiff base ligand and the complex were measured on a FTIR-650 spectrometer. ^1H NMR spectrum of the ligand was obtained using AVANCE III AV500 at 298 K. The mass spectrum (ESI) was measured on a MicroOTOF-QII. The conductivity measurement was carried out with a DDS-11 conductivity bridge. The powder XRD spectrum of the complex was recorded on a D8 Advance, and its scanning electron microscopy image was obtained using a Nova NanoSEM 200 microscope.

Synthesis of $[Zn_6Nd_2L_4(OAc)_2(DMF)EtOH]$ (1)

At room temperature, $Zn(OAc)_2 \cdot 2H_2O$ (0.20 mmol, 0.0438 g), $Nd(OAc)_3 \cdot 4H_2O$ (0.20 mmol, 0.0823 g) and H_4L (0.20 mmol, 0.0756 g) were dissolved in 20 mL MeOH, and then triethylamine in EtOH (1.0 mol L^{-1}, 2 mL) was added into the solution. The mixture was heated for 6 h under reflux with stirring, and cooled to room temperature. The clear solution was obtained by filtered, and slow diffusion of diethyl ether into the solution for one week gave the yellow crystalline product of **1**. Yield (based on $Zn(OAc)_2 \cdot 2H_2O$): 0.0302 g (35%). Mp >178 °C (decompose). EA: C, 45.06; H, 3.37; N, 5.46% (found). Calc. for $C_{97}H_{86}N_{10}Nd_2O_{32}Zn_6$: C, 45.04; H, 3.33; N, 5.42%. IR (KBr, cm^{-1}): 1578.34 (s), 1448.64 (s), 1249.94 (s), 1183.24 (s), 1083.26 (s), 879.42 (m), 788.13 (m), 839.04 (s), 731.12 (m).

Photophysical studies

The UV-vis absorbance spectra of the Schiff base ligand and the complex were determined on an UV-3600 spectrophotometer. The wavelength range is 200 nm–600 nm. The NIR emission and excitation spectra of the complex were carried out on a FLS 980 fluorimeter. Liquid nitrogen cooled Ge PIN diode detector is used to detect the NIR emissions (800 nm–1700 nm). An integrating sphere is used to obtain the quantum yield, and the luminescence lifetime is obtained by using the attached storage digital oscilloscope. Systematic errors are deducted through the standard instrument corrections.

Crystallography

The X-ray data of the complex were collected by a Smart APEX CCD diffractometer (Mo Kα radiation). The structure was solved using SHELX 97 program with direct method. The empirical absorption was corrected by SADABS program. Non-hydrogen atoms were refined anisotropically, and hydrogen atoms were calculated by geometrical methods and refined isotropically. The CCDC number of **1** is 2102148 (see www.ccdc.cam.ac.uk/data_request/cif). The bond lengths and angles are displayed in Table S1.†

For **1**: $C_{97}H_{86}N_{10}O_{32}Zn_6Nd_2$, monoclinic ($P2_1/n$), a = 20.327(15), b = 23.139(16), c = 25.376(19) Å, $\alpha = 90°$, β = 94.941(13)°, $\gamma = 90°$, V = 11 891(15) $Å^3$, $Dc = 1.444$ g cm^{-3}, μ(Mo Kα) = 2.118 mm^{-1}, T = 190 K, Z = 4, F(000) = 5176, GOF = 1.163, $R_1 = 0.0913$, $wR_2 = 0.1995$.

Conclusions

In conclusion, an octanuclear Zn(II)–Nd(III) cluster **1** was synthesized from a salen-type Schiff base ligand. The molecular sizes of **1** are 1.1 × 1.6 × 1.8 nm. It shows NIR lanthanide emission, which can be decreased gradually by the addition of Que. The emission quenching of **1** is due to the "inner filter effect" of Que. The limit of the detection of **1** to Que is 2.5 μM, and its luminescent response behaviour is not affected by the existence of some potential biomolecule interferents.

Conflicts of interest

There are no conflicts to declare.

Acknowledgements

The work was supported by the National Natural Science Foundation of China (No. 21771141).

Notes and references

1 C. Papatriantafyllopoulou, E. E. Moushi, G. Christou and A. J. Tasiopoulos, *Chem. Soc. Rev.*, 2016, **45**, 1597–1628.
2 A. Baniodeh, C. E. Anson and A. K. Powell, *Chem. Sci.*, 2013, **4**, 4354–4361.
3 Y. Ning, M. Zhu and J.-L. Zhang, *Coord. Chem. Rev.*, 2019, **399**, 213028.

4 P. Shi, H. Hu, Z. Zhang, G. Xiong and B. Zhao, *Chem. Commun.*, 2015, **51**, 3985–3988.
5 Y. Wang, G. Zhang, F. Zhang, T. Chu and Y. Yang, *Sens. Actuators, B*, 2017, **251**, 667–673.
6 Y. H. Li and W. S. Huang, *Anal. Methods*, 2015, **7**, 2537–2541.
7 Y. Zou, F. Y. Yan, T. C. Zheng, D. C. Shi, F. Z. Sun, N. Yang and L. Chen, *Talanta*, 2015, **135**, 145–148.
8 C. Y. Huang, T. K. Chen, D. M. Zhu and Q. Q. Huang, *Front. Chem.*, 2020, **8**, 225.
9 G. Chen, H. W. Zhang and J. N. Ye, *Anal. Chim. Acta*, 2000, **423**, 69–76.
10 F. Buiarelli, F. Bernardini, P. D. Filippo, C. Riccardi, D. Pomata, G. Simonetti and R. Risoluti, *Food Anal. Methods*, 2018, **11**, 3558–3562.
11 M. Arvand and M. Anvari, *J. Iran. Chem. Soc.*, 2013, **10**, 841–849.
12 D. D. Wu and Z. Chen, *Luminescence*, 2014, **29**, 307–313.
13 Y. Zou, F. Yan, L. Dai, Y. Luo, Y. Fu, N. Yang, J. Wun and L. Chen, *Carbon*, 2014, **77**, 1148–1156.
14 T.-Q. Song, K. Yuan, W.-Z. Qiao, Y. Shi, J. Dong, H.-L. Gao, X.-P. Yang, J.-Z. Cui and B. Zhao, *Anal. Chem.*, 2019, **91**, 2595–2599.
15 W.-K. Wong, H. Liang, W.-Y. Wong, Z. Cai, K.-F. Li and K.-W. Cheah, *New J. Chem.*, 2002, **26**, 275–278.
16 Y.-X. Chi, S.-Y. Niu, J. Jin, R. Wang and Y. Li, *J. Chem. Soc., Dalton Trans.*, 2009, **47**, 7653–7659.
17 S. G. Baca, H. Adams, C. S. Grange, A. P. Smith, I. Sazanovich and M. D. Ward, *Inorg. Chem.*, 2007, **46**, 9779–9789.
18 H.-B. Xu, L.-X. Shi, E. Ma, L.-Y. Zhang, Q.-H. Wei and Z.-N. Chen, *Chem. Commun.*, 2006, 1601–1603.
19 S. Torelli, D. Imbert, M. Cantuel, G. Bernardinelli, S. Delahaye, A. Hauser, J.-C. G. Bünzli and C. Piguet, *Chem.–Eur. J.*, 2005, **11**, 3228–3242.
20 W.-K. Wong, X.-J. Zhu and W.-Y. Wong, *Coord. Chem. Rev.*, 2007, **251**, 2386–2399.
21 J. Zhang, L. Xu and W.-Y. Wong, *Coord. Chem. Rev.*, 2018, **355**, 180–198.
22 C. Wang, X. Yang, S. Wang, T. Zhu, L. Bo, L. Zhang, H. Chen, D. Jiang, X. Dong and S. Huang, *J. Mater. Chem. C*, 2018, **6**, 865–874.
23 D. Jiang, X. Yang, X. Zheng, L. Bo, T. Zhu, H. Chen, L. Zhang and S. Huang, *J. Mater. Chem. C*, 2018, **6**, 8513–8521.
24 D. Shi, X. Yang, Z. Xiao, X. Liu, H. Chen, Y. Ma, D. Schipper and R. A. Jones, *Nanoscale*, 2020, **12**, 1384–1388.
25 Y. Ma, X. Yang, M. Niu, D. Shi and D. Schipper, *J. Lumin.*, 2022, **241**, 118494.
26 F. Lam, J.-X. Xu and K.-S. Chan, *J. Org. Chem.*, 1996, **61**, 8414–8418.
27 V. Chandrasekhar, A. Athimoolam, N. D. Reddy, S. Nagendran, A. Steiner, S. Zacchini and R. Butcher, *Inorg. Chem.*, 2003, **42**, 51–59.
28 A. M. Rahman, R. Bishop, D. C. Craig and M. L. Scudder, *CrystEngComm*, 2003, **5**, 422–428.
29 W. K. Wong, X. Yang, R. A. Jones, J. Rivers, V. Lynch, W. K. Lo, D. Xiao, M. M. Oye and A. Holmes, *Inorg. Chem.*, 2006, **45**, 4340–4345.
30 S. I. Klink, L. Grave, D. N. Reinhoudt and F. C. J. M. v. Veggel, *J. Phys. Chem. A*, 2000, **104**, 5457–5468.
31 J.-C. G. Bünzli and C. Piguet, *Chem. Soc. Rev.*, 2005, **34**, 1048–1077.
32 Y. Xiao, Y. Cui, Q. Zheng, S. Xiang, G. Qian and B. Chen, *Chem. Commun.*, 2010, **46**, 5503–5505.
33 X. Qi, Y. Jin, N. Li, Z. Wang, K. Wang and Q. Zhang, *Chem. Commun.*, 2017, **53**, 10318–10321.
34 H.-W. Yang, P. Xu, B. Ding, X.-G. Wang, Z.-Y. Liu, H.-K. Zhao, X.-J. Zhao and E.-C. Yang, *Cryst. Growth Des.*, 2020, **20**, 7615–7625.
35 Z.-X. Wang, Y.-F. Gao, X. Jin, X.-H. Yu, X. Tao, F.-Y. Kong, D.-H. Fan and W. Wang, *Analyst*, 2019, **144**, 2256–2263.
36 C. Li, W. Liu, X. Sun, W. Pan, G. Yu and J. Wang, *Sens. Actuators, B*, 2018, **263**, 1–9.
37 H. Qiu, C. Luo, M. Sun, F. Lu, L. Fan and X. Li, *Food Chem.*, 2012, **134**, 469–473.
38 J.-C. G. Bünzli and C. Piguet, *Chem. Soc. Rev.*, 2005, **34**, 1048–1077.
39 S. Xu, J. Shi, B. Ding, Z. Liu, X. Wang, X. Zhao and E. Yang, *Dalton Trans.*, 2019, **48**, 1823–1834.
40 F. Zhang, H. Yao, T. Chu, G. Zhang, Y. Wang and Y. Yang, *Chem.–Eur. J.*, 2017, **23**, 10293–10300.
41 Y. Zhang, B. Li, H. Ma, L. Zhang, H. Jiang, H. Song, L. Zhang and Y. Luo, *J. Mater. Chem. C*, 2016, **4**, 7294–7301.